Influence of spreader geometries on powder bed quality with rough substrate surfaces in laser powder bed fusion process

Wu, Yaping; Chu, Fuzhong; Zhang, Chaocai; Yan, Hongyu; Wang, Lin; Zhou, Zongyan

DOI
10.1016/j.partic.2025.07.007

Publication date
2025

Document Version
Final published version

Published in
Particuology

Particuology 104 (2025) 289–301

Contents lists available at ScienceDirect

Particuology

journal homepage: www.elsevier.com/locate/partic

Influence of spreader geometries on powder bed quality with rough substrate surfaces in laser powder bed fusion process

Yaping Wu [a,b], Fuzhong Chu [c], Chaocai Zhang [a,b], Hongyu Yan [a,b], Lin Wang [d], Zongyan Zhou [a,b,c,*]

[a] Jiangxi Provincial Key Laboratory of Particle Technology, Jiangxi University of Science and Technology, Nanchang, 330013, China
[b] Research Centre for Intelligent Mineral Processing & Metallurgy, Jiangxi University of Science and Technology, Nanchang, 330013, China
[c] ARC Research Hub for Smart Process Design and Control, Department of Chemical and Biological Engineering, Monash University, Melbourne, VIC, 3800, Australia
[d] Resource & Recycling, Department of Engineering Structures, Faculty of Civil Engineering and Geosciences, Delft University of Technology, 2628 CN, Delft, the Netherlands

ARTICLE INFO

Article history:
Received 25 January 2025
Received in revised form
2 May 2025
Accepted 9 July 2025
Available online 16 July 2025

Keywords:
Discrete element method
Spreader geometry
Laser powder bed fusion
Powder spreading
Surface roughness

ABSTRACT

The quality of parts manufactured by laser powder bed fusion is closely related to the uniformity and density of the powder bed. In this work, the discrete element method is used to simulate the powder spreading process by different spreader geometries with rough substrate surfaces. The results indicate that reducing the spreader inclination angle significantly increases the number of force chains, enhances compaction, and consequently improves the quality of the powder bed. Studies also show that optimizing the bottom structure of the spreader can effectively reduce exposed areas. An arc-shaped structure promotes particle packing and filling, improving the powder distribution characteristics. A narrow spreader significantly affects the packing density of the powder bed at low layer gaps, whereas a wide spreader is relatively less constrained. At high spreading speeds, the spreader with an inclination angle of 135° produces the highest quality of the powder bed. R1000 performs excellently at larger layer gaps. The above findings provide valuable guidance for optimizing powder spreading strategies in the laser powder bed fusion process.

1. Introduction

Laser powder bed fusion (LPBF), as an important process in additive manufacturing, has gained significant attention for its capability to produce high-precision and high-performance components. It is widely applied in aerospace, biomedical, and automotive manufacturing industries (Bremen et al., 2012; Ngo et al., 2018; Zhao et al., 2022). The core principle of the LPBF process is to use a high-energy laser beam to selectively melt metal powder layer by layer on the powder bed, thereby constructing the desired components (Khairallah et al., 2016; Murr et al., 2012). The quality of the powder bed is critical to the LPBF process, as its uniformity and density directly influence the laser melting efficiency and the stability of part performance (Ali et al., 2022; Qin et al., 2024; Wang et al., 2023).

During the LPBF process, various factors influence the quality of powder beds, including particle-related properties (e.g., size distribution, powder morphology, and adhesions), operation-related parameters (e.g., powder spreading speed, layer thickness, and spreader shape), and substrate-related characteristics (Cao et al., 2021; Miao et al., 2022; Salehi et al., 2023). Among these factors, the geometry of the spreader, as a key operational parameter, has a significant impact on powder distribution and flow behavior (Phua et al., 2021). Spreader with different geometries (such as roller or spreader) vary in contact angle, edge shape, and interaction mode with the powder, leading to differences in the characteristics of powder layer regarding to thickness, surface roughness, and density (Gao et al., 2024; Sehhat & Mahdianikhotbesara, 2021). In recent years, the impact of spreader geometries on powder

* Corresponding author. Jiangxi Provincial Key Laboratory of Particle Technology, Jiangxi University of Science and Technology, Nanchang, 330013, China.
E-mail address: zongyan.zhou@jxust.edu.cn (Z. Zhou).

https://doi.org/10.1016/j.partic.2025.07.007

spreading quality has garnered increasing attention. Nan and Gu (2020) found that roller-based spreading results in a smaller total particle volume than spreader-based spreading, and it is more sensitive to variations in particle surface energy. Cao (2019) further pointed out that compared to vertical and chamfered spreaders, non-rotating roller spreading achieves the highest packing density and the best bed uniformity. Furthermore, Wang et al. (2021, 2022) found that compared to vertical spreaders, spreaders with curved or inclined surfaces can deposit more particles within a compact space, while rollers perform better at larger layer gaps. This is because smaller inclination angles and larger curvature radius help create a buffer zone to store powder, ensuring uniform spreading while reducing particle collisions. Regarding the effect of spreader inclination angle, Li et al. (2024) discovered that when the spreader inclination angle is less than 90°, the packing density of the powder bed decreases with increasing inclination angle, while the surface roughness first decreases and then slightly increases as the inclination angle grows. Similarly, Yao et al. (2021) observed that the packing density and uniformity of the powder bed exhibit a trend of initially increasing and then decreasing with the increase in spreader angle. In addition, Li et al. (2020) found that compared to double-cylinder spreaders, super-elliptical spreaders increase the contact area, reduce disturbance and dilatancy effects, and effectively improve the quality of the powder bed. Meanwhile, Haeri (2017) and Wu et al. (2022) further improved powder bed quality by optimizing the geometric design of spreader profiles, providing new directions for spreader design optimization.

The studies shown above indicate that the types of spreaders and their design parameters (such as spreader inclination angle) have a significant impact on powder spreading behavior. However, these studies primarily analyze the influence patterns and underlying mechanisms of powder spreading performance based on smooth substrate surfaces. In practice, the substrate surface where powder deposit is generated from the melting and solidification of previous powder layer, hence it might display various roughness (Chu et al., 2023). The interactions of different spreaders on rough substrate surfaces require further in-depth investigation. Therefore, this study employs the discrete element method to quantitatively investigate the powder spreading performance of different spreader geometries under rough substrate conditions. The study focuses on analyzing the effects of the geometric characteristics of spreader and operational parameters on powder spreading behavior in terms of powder bed packing density, uniformity, and particle flow behavior. By comparing the performance of different spreaders under rough substrate conditions, this study provides a theoretical foundation for the design optimization of spreaders and the improvement of additive manufacturing process.

2. Model description and simulation conditions

2.1. DEM

Discrete element method (DEM) (Cundall & Strack, 1979; Tsuji et al., 1992) is a numerical approach used to simulate the dynamic behavior of particulate systems by tracking the motion of individual particles within the system. In the DEM, the interaction forces between particles mainly consist of normal and tangential viscoelastic contact forces, friction, and cohesive forces, such as van der Waals force. The motion of particles is divided into translational and rotational components, governed by Newton's second law:

$$m_i\frac{d\mathbf{v}_i}{dt}=\sum_{j=1}^{k_c}\left(\mathbf{f}_{c,ij}+\mathbf{f}_{d,ij}\right)+m_i\mathbf{g} \tag{1}$$

$$\mathbf{I}_i\frac{d\boldsymbol{\omega}_i}{dt}=\sum_{j=1}^{k_c}\left(\mathbf{M}_{t,ij}+\mathbf{M}_{r,ij}\right) \tag{2}$$

where $\mathbf{v}_i$ and $\boldsymbol{\omega}_i$ represent translational and rotational velocities of the particle i respectively, and k_c is the number of particles interacting with particle i. The simulated forces include the particle weight $m_i\mathbf{g}$, and inter-particle forces, such as elastic contact force $\mathbf{f}_{c,ij}$, viscous damping force $\mathbf{f}_{d,ij}$. These contact forces are resolved into normal components and tangential components. The torque acting between particle i and particle j is divided into rotational torque ($\mathbf{M}_{t,ij}$) and rolling friction torque ($\mathbf{M}_{r,ij}$). $\mathbf{M}_{t,ij}$ is induced by tangential forces, causing particle i to rotate, while $\mathbf{M}_{r,ij}$ is generated by rolling friction, opposing the relative rotation of particle i.

The contact forces between particles are typically described by the Hertz-Mindlin contact model (Hertz, 1882; Mindlin, 1949; Mindlin & Deresiewicz, 1953), which decomposes the contact force into normal and tangential components, corresponding to the elastic deformation and frictional properties of the particles, respectively. The normal force is based on Hertzian contact theory, reflecting the force generated by elastic deformation during particle contact. Note that the normal contact force must also account for the adhesive forces between powder particles. This study employs the van der Waals force model based on Hamaker theory to describe particle adhesion. Van der Waals force, an intrinsic attractive force between materials, can be calculated using the following equation (Hamaker, 1937; Lifshitz & Hamermesh, 1992):

$$\mathbf{F}_v=-\frac{H}{6}\left[\frac{2r_ir_j}{d^2-\left(r_i+r_j\right)^2}+\frac{2r_ir_j}{d^2-\left(r_i-r_j\right)^2}+ln\left(\frac{d^2-\left(r_i+r_j\right)^2}{d^2-\left(r_i-r_j\right)^2}\right)\right] \tag{3}$$

where H is the Hamaker constant, which determines the magnitude of the force, and d is the distance between the centers of particles i and j. When the closest distance between the surfaces of two particles exceeds 1 μm, the van der Waals force becomes negligible as it is several orders of magnitude smaller than gravity and is thus excluded from this simulation.

2.2. Simulation conditions

In this work, the particles used are Ti-6Al-4V (TC4) titanium alloy powders, with their actual morphology shown in Fig. 1(a). Considering that highly spherical powders prepared via gas atomization are commonly used in LPBF, the particle shape is assumed spherical in this work (Chen et al., 2019; Roy et al., 2024). The particle size distribution of the TC4 powders is shown in Fig. 1 (b). In this study, multiple spreaders were designed, as shown in Fig. 1(c). All spreaders have a height of 2000 μm. Spreaders A to E have inclination angles of 30°, 45°, 90°, 120°, and 135°, respectively. All spreaders share the same width and a length of 50 μm. Spreaders F to H are structurally modified based on the vertical spreader (C). The bottom of spreader F has a length of 20 μm along the x-direction, while spreaders G and H feature an arc-shaped bottom design with radii of 30 μm and 60 μm, respectively. Spreaders I to L are designed by increasing the thickness of spreaders C and F to H, aiming to examine the effect of spreader thickness on powder spreading performance. Among them, the bottom of spreader J has a length of 1000 μm along the x-direction,

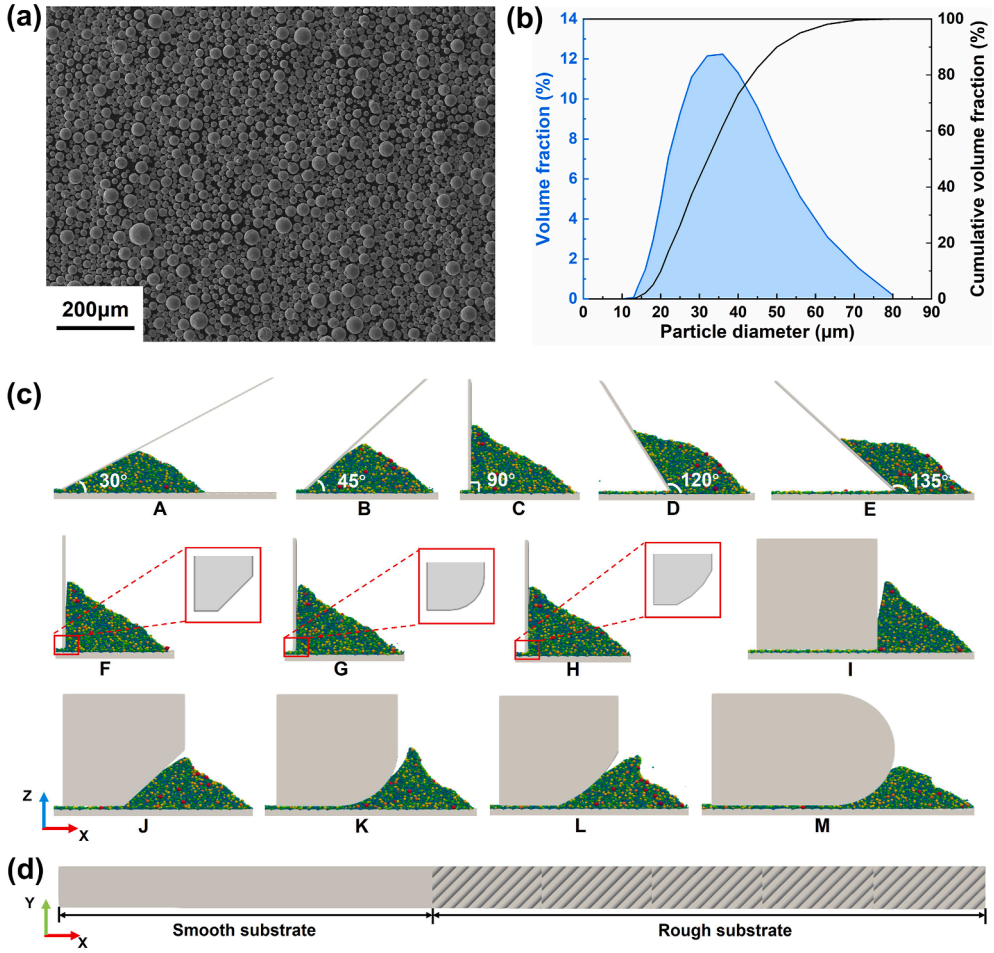

Fig. 1. (a) SEM image of Ti-6Al-4V powder; (b) particle size distribution of the powder used in the simulation; (c) spreaders A–E correspond to 30°, 45°, 90°, 120°, and 135°; spreaders F–H correspond to cut-blade, R30, and R60; spreaders I–M correspond to wideblade, cut-wideblade, R1000, R2000, and half-roundblade, respectively; (d) powder spreading substrate illustration (Note that the substrate roughness of the rough region was characterized using the maximum peak height S_p, which is $S_p = 60$ μm in this model).

while spreaders K and L feature an arc-shaped bottom design with radii of 1000 μm and 2000 μm, respectively. Spreader M is a semi-circular spreader with a radius of 1000 μm.

The powder spreading substrate used in this study is divided into smooth and rough regions, as shown in Fig. 1(d). The smooth region is located at the front of the substrate, while the rough region at the rear simulates the solid-state forming zone. The rough substrate features a surface texture with an angle of 45° relative to the powder spreading direction. The TC4 particle parameters used in the simulation (He et al., 2021) are shown in Table 1. In the process of material parameter calibration, the angle of repose serves as a key indicator for evaluating the rationality of powder parameters and the validity of the model. Using the powder deposition simulation method proposed by Wang et al. (2020), this work obtained an angle of repose of 25°. Compared to the reported range of 24°–29° in the literature (He et al., 2021; Meier et al., 2019), the simulated result falls within a reasonable range, demonstrating the rationality and validity of the constructed particle model and selected material parameters.

Table 1
TC4 powder parameters used in the simulation.

Parameter	Value
Particle size, d	13–80 μm
Particle density, ρ	4430 kg/m^3
Coefficient of sliding friction, μ_s	0.3
Coefficient of rolling friction, μ_r	0.01
Young's modulus, Y	1.1 ×10^8 Pa
Coefficient of restitution, e	0.4
Poisson's ratio, ν	0.3
Hamaker constant, H	1.2 ×10^{-20} J
Time step	0.005 μs
Spreading speed	0.025–0.15 m/s
Layer gap	120–250 μm

2.3. Powder layer characterization

The powder layer characteristics are presented by packing density and uniformity in this work. As shown in Fig. 2, a cubic region is set 500 μm away from the fixed spreader to calculate the packing density (ρ) of the particles within this region. The packing density is defined as the ratio of the particle volume to the cube volume ($\rho = V_{particles}/V_{cube}$). By continuously collecting data during the movement of the spreader, the average packing density ρ_{avg}, which reflects the powder layer's compactness, and the coefficient of variation φ_{vc}, which characterizes the powder layer's uniformity, are calculated. The corresponding formulas are as follows:

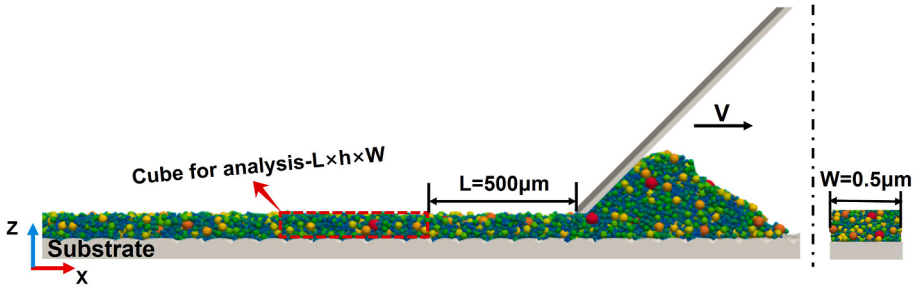

Fig. 2. Schematic diagram of the cubic region used to quantify powder layer characteristics during the powder spreading process.

$$\begin{cases} \rho_{avg} = \dfrac{\sum_{i=0}^{n}\rho_i}{n} \\ \varphi_{vc} = \dfrac{\varphi_{st}}{\rho_{avg}} \end{cases} \tag{4}$$

where n represents the number of packing density ρ measurements collected during data acquisition, and φ_{st} denotes the standard deviation of the average packing density φ_{avg}. These two indicators are commonly used to describe the macroscopic packing characteristics of the powder layer (Si et al., 2021). In general, a larger φ_{avg} and a smaller φ_{vc} indicate that the powder layer has higher density and better uniformity (Yao et al., 2021).

3. Results and discussion

3.1. Effect of spreader geometries on powder distribution

Fig. 3 shows the top-view simulation results of powder spreading under different spreaders conditions. On a smooth surface, the top view does not clearly indicate which spreader achieves the best spreading performance. On the rough surface, it can be observed that for spreaders A–E, as the spreader inclination angle increases, a large number of void defects appear in the powder bed. Spreaders F–H, due to the adjustments in their bottom structure, show some improvement in reducing exposed areas on the substrate surface compared to spreader C. Spreaders I–M, through the optimization of the wide spreader bottom structure, significantly enhance the powder bed packing performance.

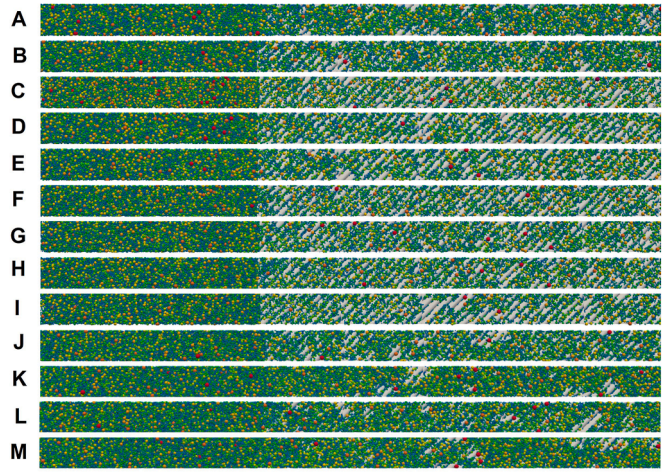

Fig. 3. Comparison of spreading results for different spreaders: spreaders A–E correspond to 30°, 45°, 90°, 120°, and 135°; spreaders F–H correspond to cut-blade, R30, and R60; spreaders I–M correspond to wideblade, cut-wideblade, R1000, R2000, and half-roundblade.

To visually illustrate the variation in powder coverage within the rough region, we conducted a quantitative analysis of the uncovered areas in the powder bed. Figs. 4(a1)-(a3) show the proportion of exposed area in the rough region relative to the entire area in each powder bed. As shown in the figure, as the spreader inclination angle increases from 30° to 120°, the exposed area fraction rises from 14.4 % to 33.7 %. When the angle further increases to 135°, the exposed area fraction slightly decreases to 30.8 %. For narrow spreaders such as 90°, cut-blade, R30, and R60, the exposed area fraction gradually decreases from 31.8 % to 26.9 %. Additionally, the exposed area fraction for the wide spreader (wideblade) is 1.5 % higher than that of the narrow spreader (90°). However, by optimizing the bottom structure of the wide spreader (e.g., cut-wideblade, R1000, and R2000), the exposed area fraction can be significantly reduced to 9 %. Among all spreaders, the half-roundblade exhibits the best performance, with an exposed area fraction of only 8.5 %.

The coordination number distribution is an important indicator of the compactness of the powder layer. For any given metal particle, the coordination number refers to the number of other particles in direct contact with it (Xiang et al., 2016). Generally, a higher coordination number indicates a denser packing of the powder layer, thereby reducing the likelihood of defects during the printing process. Figs. 4(b1)-(b3) show the impact of different spreaders on the particle coordination number distribution. As seen in Fig. 4(b1), the coordination number distribution for 30° is slightly skewed to the right and is more concentrated, indicating that the particle packing is denser, resulting in a smaller exposed area. In contrast, the coordination number peaks for other spreaders shift to the left, indicating reduced particle contact and less compact packing. In Fig. 4(b2), the coordination number distributions for 90°, cut-blade, R30, and R60 are quite similar, indicating that the powder beds formed by these spreaders have similar particle packing densities. Fig. 4(b3) shows that the coordination number distributions for wideblade and cut-wideblade are clearly shifted to the left, suggesting fewer particle contacts and looser packing, resulting in a larger exposed area. In contrast, the coordination number distributions for R1000, R2000, and half-roundblade are more concentrated, indicating increased particle contacts and denser packing, which significantly reduces the exposed area. Particularly, the half-roundblade has the most concentrated coordination number distribution, the densest particle packing, and thus the lowest exposed area.

The powder deposition on the smooth surfaces for different spreaders is also examined, and the results are shown in Fig. 5. It can be observed that spreaders K and M achieve the highest powder deposition per unit area. As the spreader inclination angle increases, the powder deposition decreases when the angle is below 90°, increases after exceeding 90°, with a slight decline

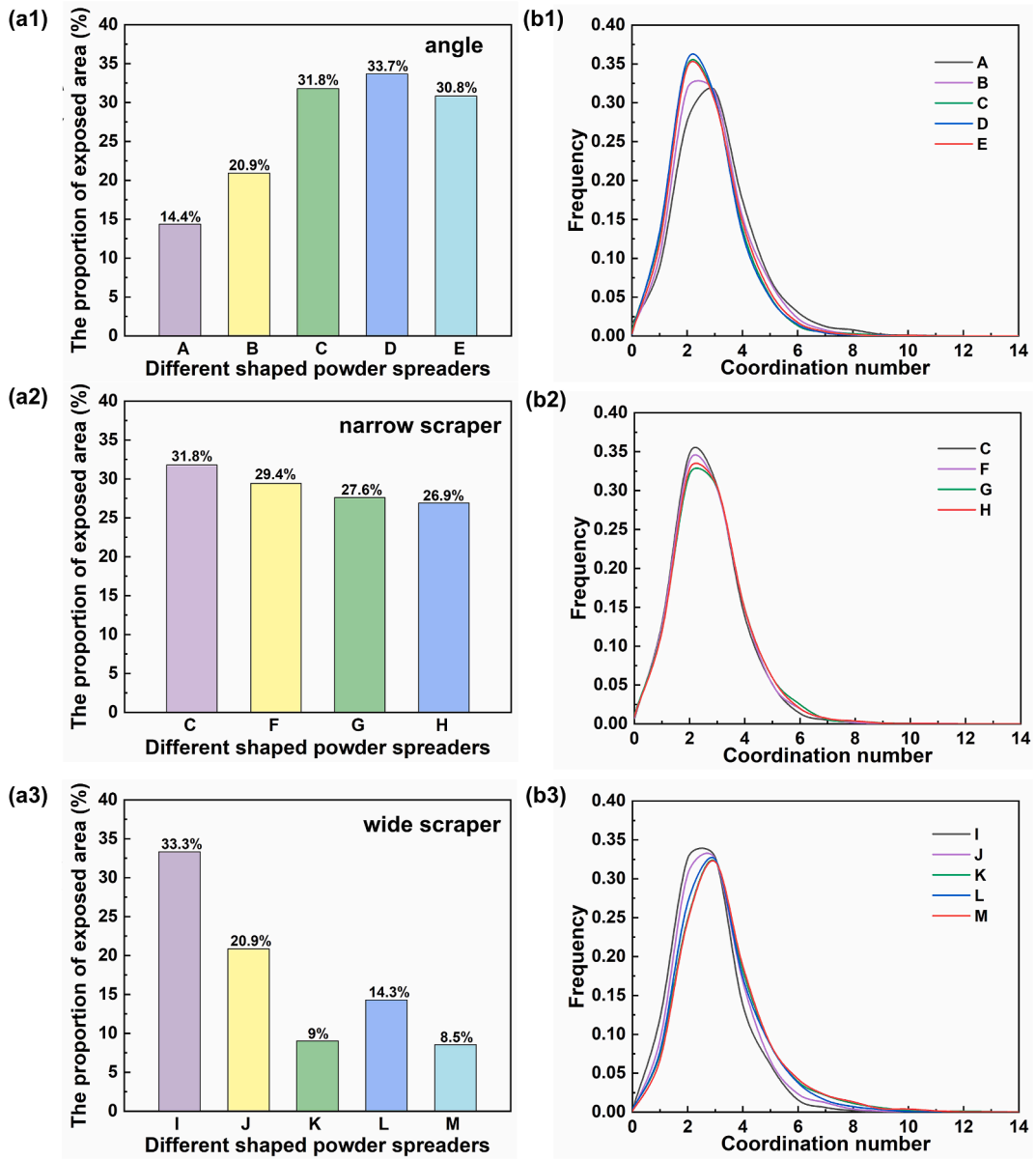

Fig. 4. (a1)–(a3): Proportion of exposed area in the powder layer within the rough region for different spreaders; (b1)–(b3): Effect of different spreaders on coordination number distribution (spreaders A–E correspond to 30°, 45°, 90°, 120°, and 135°; spreaders F–H correspond to cut-blade, R30, and R60; spreaders I–M correspond to wideblade, cut-wideblade, R1000, R2000, and half-roundblade).

observed at an inclination angle of 135°. Narrow spreaders (C, F–H) somewhat increase the powder deposition, but the effect is more significant with the wide spreaders (I–L).

Overall, regardless of whether on smooth or rough substrate surfaces, the powder bed quality generated by spreaders A, K, L, and M is superior to that of the other tools.

In addition, representative spreaders (e.g., 90° (C), R30 (G), and R1000 (K)) were selected to investigate the effect of substrate roughness on the quality of the powder bed. Fig. 6 illustrates the top views of the powder beds generated by the three spreaders with the roughness of 10 μm and 30 μm. Combined with Fig. 3, it can be seen that when the substrate roughness increases from 0 μm to 30 μm, a small amount of bare areas appear for spreaders 90° and R30, resulting in a decrease of the bed quality. With the roughness further increasing to 60 μm, a large percentage of bare areas appear for all the three spreaders, but the percentage of bare areas by R1000 is significantly lower than that of the other two. In order to better evaluate the performance of different spreaders, subsequent studies will focus on the substrate with a roughness of 60 μm and explore the effect of different spreaders on the powder bed quality.

3.2. Effect of spreader geometries on particle velocity

During the powder spreading process, the spreader directly acts on the powder particles, and its shape influences the force state of the powder, thereby affecting the flow and distribution characteristics of the particles. This directly impacts the uniformity and density of the powder bed (Penny et al., 2024). The velocity vector distribution of particles under different spreader conditions is shown in Fig. 7. To visually illustrate the movement of particles in the powder bed under different conditions, we

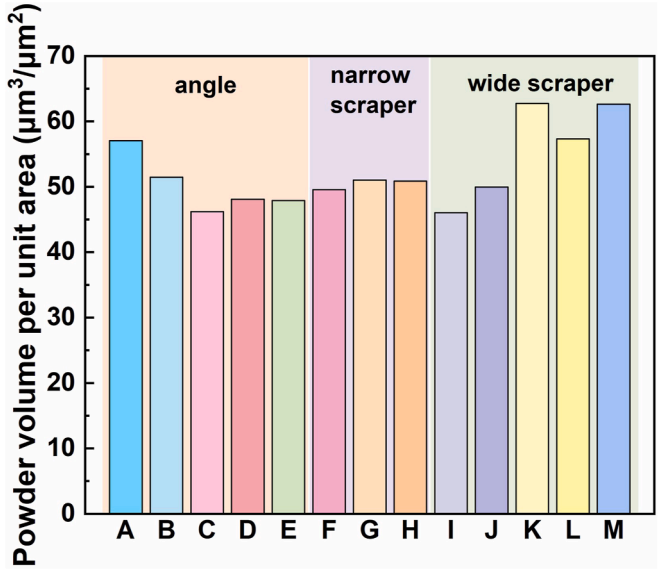

Fig. 5. Influence of spreader geometry on the volume of particles deposited onto a smooth surface: spreaders A–E correspond to 30°, 45°, 90°, 120°, and 135°; spreaders F–H correspond to cut-blade, R30, and R60; spreaders I–M correspond to wideblade, cut-wideblade, R1000, R2000, and half-roundblade.

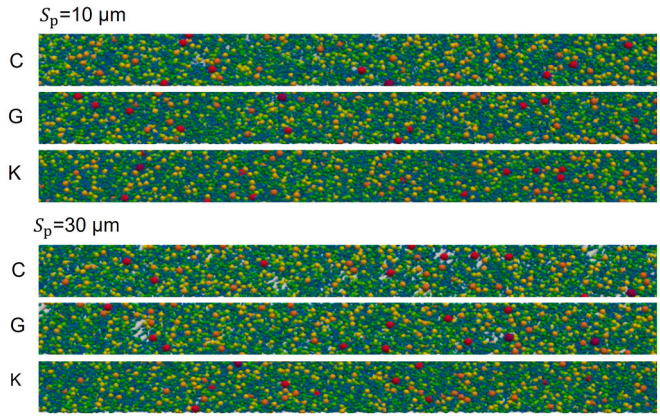

Fig. 6. Top view of the powder bed generated by the spreaders C (90°), G (R30) and K (R1000) with roughness of 10 μm and 30 μm.

employed the method used in Wang et al.'s work (2021), which involves subtracting the spreading speed from the particle velocity along the spreading direction. Different colors in the figure represent the magnitude of the velocity. As shown in the figure, significant particle circulation is observed in the powder beds corresponding to spreaders 30°, 45°, cut-wideblade, R1000, R2000, and half-roundblade. This circulation facilitates the redistribution of particles on the rough surface, thereby covering the substrate more effectively. For the 135° spreader, the movement trend of the particles shows a downward inclination. This is due to the larger inclination angle of the 135°, which results in a relatively smaller lateral pressure applied to the particles. The larger angle makes it easier for particles to slide rather than form rotational flow. Additionally, it can be observed that the particle movement direction in the central region of the powder bed is approximately aligned with the texture direction of the rough substrate surface, at a 45° angle (using spreader A as an example). However, when the spreader inclination angle is sufficiently large (e.g., 135°), this movement trend is completely eliminated.

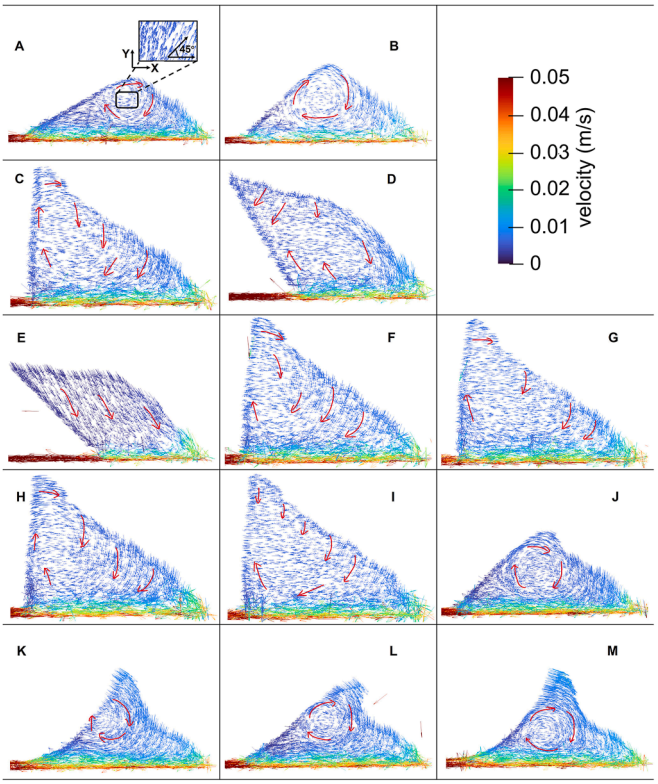

Fig. 7. Particle velocity vector distribution at a specific moment during the powder spreading process under different spreader conditions (spreaders A–E correspond to 30°, 45°, 90°, 120°, and 135°; spreaders F–H correspond to cut-blade, R30, and R60; spreaders I–M correspond to wideblade, cut-wideblade, R1000, R2000, and half-roundblade).

3.3. *Effect of spreader geometries on particle dynamics*

To comprehensively explore the impact of spreader geometry on particle motion and distribution, we further analyzed the interaction forces between particles and the rough substrate, between particles and the spreader, and among particles. The variation patterns of these forces provide deeper theoretical insights into powder spreading efficiency and uniformity.

Fig. 8 shows the average contact force between particles and the substrate surface over time for different spreaders. It can be observed that for spreaders with different inclination angles (30°–135°) (Fig. 8(a)), the force fluctuations increase significantly, particularly when the spreader is inclined. Compared to the vertical spreader at 90°, the force fluctuations are more pronounced. This phenomenon is closely related to the influence of spreader angle on particle motion and packing behavior. Inclined spreaders introduce a horizontal component of force, altering the particle movement pattern. Compared to vertical spreaders, inclined spreaders cause particles to slide or roll along the spreader's inclined direction rather than directly forming a uniform accumulation on the substrate. This sliding behavior results in frequent changes in particle-substrate contact points, thereby intensifying the fluctuations in contact force. Additionally, the obstructive effect of the rough substrate on particle flow is amplified under the action of the inclined spreader. Sliding particles may experience momentarily large contact forces due to collisions and blockages with the substrate surface. As seen in the figure, when the spreader inclination angle is 135°, the force fluctuations are particularly frequent, further validating the influence of spreader angle on force fluctuations.

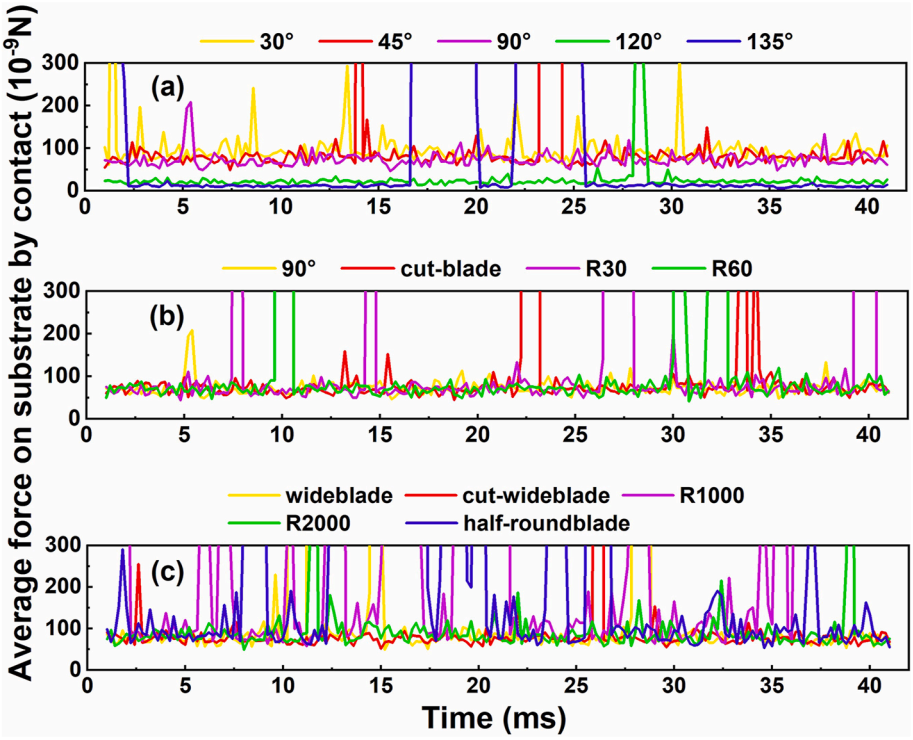

Fig. 8. Average contact force between particles and the substrate surface: (a) spreaders with different inclination angles, (b) narrow spreaders, and (c) wide spreaders.

Adjusting the bottom structure of the vertical spreader (90°) (e.g., cut-blade, R30, and R60) also significantly alters the powder spreading path and deposition behavior of the particles (Fig. 8(b)). The modified spreaders increase the contact points between particles and substrates, making the local collisions and force propagation paths more complex. At the same time, the rolling and sliding actions of the particles are enhanced, leading to more frequent interactions between the particles and the substrate. This results in a more complex distribution of contact forces, significantly increasing the fluctuations in the average contact force.

When the spreader thickness increases (e.g., cut-wideblade and R2000) (Fig. 8(c)), this effect is somewhat suppressed. Due to the larger contact area of the wide spreader, the particle deposition area becomes more extensive, and the distribution is more uniform. The contact points between the particles and the substrate are more numerous and distributed more evenly, reducing localized accumulation or sliding. This results in smaller fluctuations in the contact force between the particles and the substrate. The wide spreader can transmit forces more evenly across the entire contact area, preventing excessive local contact forces. Additionally, bottom circular structures (e.g., R1000 and half-roundblade) amplify this effect because the circular design causes particles to concentrate in specific locations, creating higher localized pressure. When particles slide or rearrange under the pushing of spreaders, the contact forces in these localized areas can rapidly increase, leading to greater fluctuations in the contact force. From the figure, it can be observed that the contact force between particles and the substrate should not be too small, as this would prevent the particles from tightly adhering to the substrate surface, leading to an increase in particle gaps. During the deposition process, particles are more likely to slide or redistribute, resulting in an increased area of uncovered regions, which reduces the performance of the powder bed.

Fig. 9 shows the average contact force between particles and spreader surfaces over time on rough substrates. It can be observed that the contact force applied by certain spreaders significantly increases at specific moments. Taking the 135° inclined spreader in Fig. 9(a) as an example, the inserted figure shows the distribution of average contact force between the spreader and particles at t = 18.6 ms. The reason for the large forces observed at certain moments is that when the spreader applies pressure to the particles, the particles come into contact with each other and begin to accumulate. If the gap between the lower end of the spreader and the substrate is small, particles tend to accumulate in localized areas and become trapped, leading to a sharp increase in localized pressure. This accumulation effect not only causes particle blockage, further increasing resistance, but also manifests as a sharp rise in contact force. Additionally, although smaller particles typically flow more easily during the spreading process, they may also accumulate in localized areas between the spreader and the substrate. When a large number of small particles gather, they can increase the surface area of the contact region, leading to higher localized pressure. Furthermore, by filling voids, these small particles may induce blockage of larger particles, exacerbating the increase in contact force.

During the powder spreading process, the variation in contact force between particles and the spreaders not only reflects the particle packing and flow behavior but may also lead to potential issues. Excessive contact force between the particles and the spreader can accelerate tool wear, especially during particle accumulation, blockage, and force concentration. This high-intensity contact force is prone to causing edge wear, dulling, or even cracking, thereby shortening the tool's lifespan. At the same time, the peak contact force may lead to particle accumulation, causing uneven powder spreading, which in turn affects the density, surface finish, and structural performance of the printed part. Moreover, excessively compacted particles can result in uneven

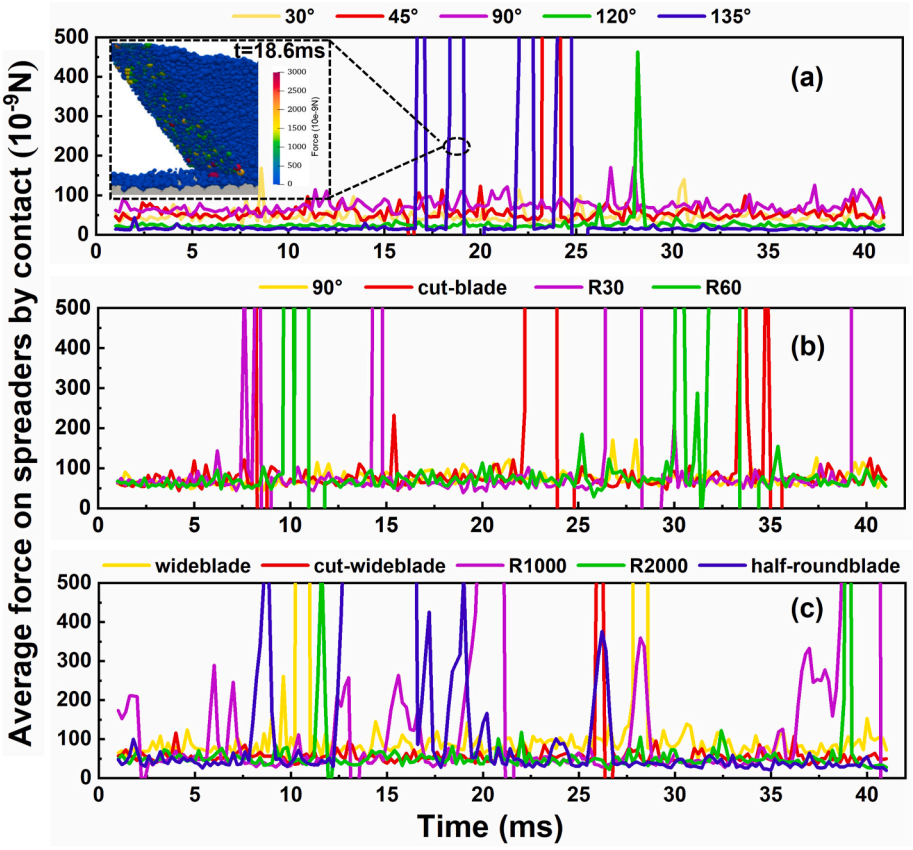

Fig. 9. Average contact force between particles and the surface of the spreaders: (a) spreaders with different inclination angles, (b) narrow spreaders, and (c) wide spreaders.

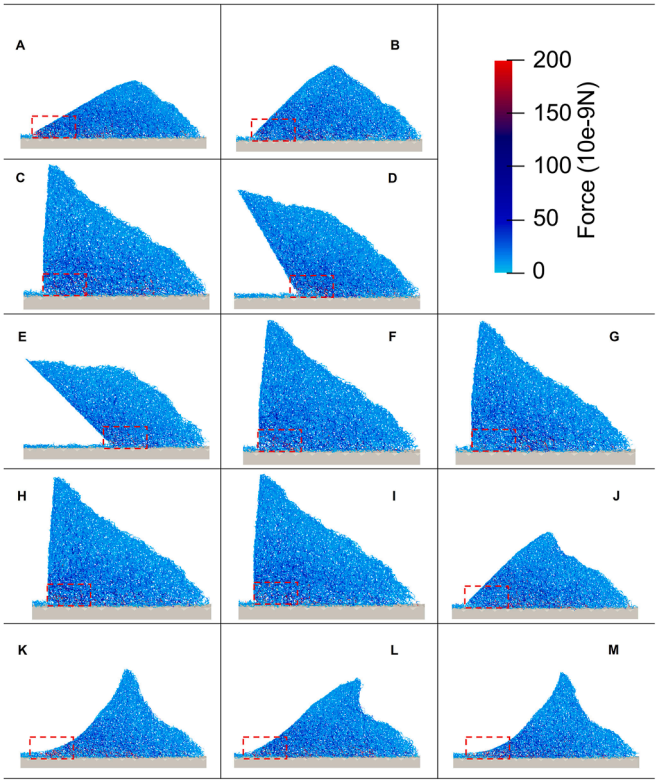

Fig. 10. Force chain diagram between particles (Spreaders A–E correspond to 30°, 45°, 90°, 120°, and 135°; spreaders F–H correspond to cut-blade, R30, and R60; spreaders I–M correspond to wideblade, cut-wideblade, R1000, R2000, and half-roundblade).

material layer thickness, reducing the accuracy and mechanical properties of the finished product. Therefore, from Fig. 9(a), it can be observed that the 30° (spreader A) and 90° (spreader C) spreaders exhibit relatively higher stability in contact force. Combined with the analysis results from Figs. 4(a1)-(a3), it can be further confirmed that the 30° spreader performs optimally in reducing contact force fluctuations and improving powder spreading uniformity. For narrow spreaders (Fig. 9(b)), the changes in the bottom structure lead to frequent fluctuations in the average contact force between the spreader and the particles. Increasing the spreader's thickness produces similar effects, as shown in Fig. 9(c), where R1000 and half-roundblade exhibit more pronounced force fluctuations. Compared to straight shapes, curved spreaders compress and release particles periodically during movement, causing the accumulation pressure to be released suddenly, which results in larger force fluctuations.

Fig. 10 shows the distribution of normal contact force chains between particles, with different colors representing the magnitude of the force. It can be observed that strong force chains are mainly concentrated in the gap area in front of the spreader. During the powder spreading process, as the particles move, the force chains continuously break and reform, causing the contact force in the powder bed to change dynamically.

To more intuitively observe the variation in inter-particle forces, Fig. 11 presents the curve of the average contact force between particles over time on a rough surface. In Fig. 10, the red dashed line marks the computational region of the study, which is approximately 500 μm in length and 250 μm in width. From Fig. 10, it can be observed that when the spreader inclination angle is small (e.g., 30° and 45°), the force applied by the spreader to the particles is larger, causing significant compression and

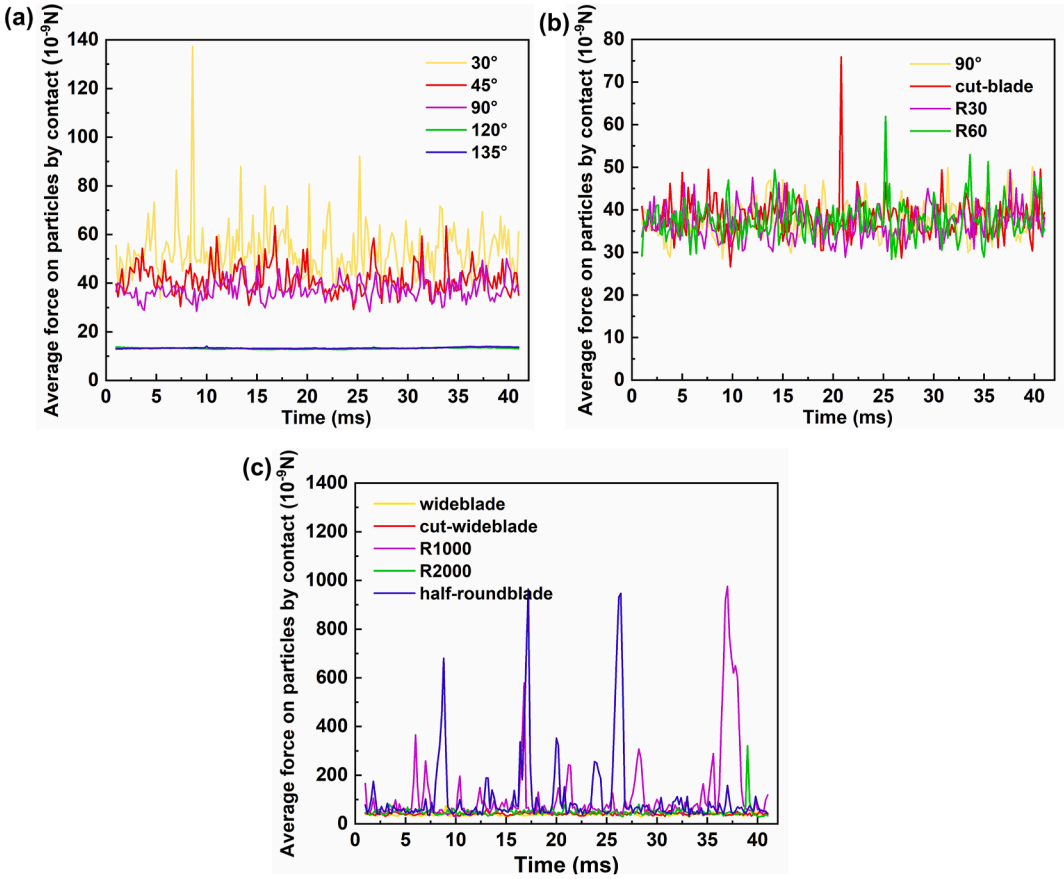

Fig. 11. Average contact force between particles: (a) spreaders with different inclination angles, (b) narrow spreaders, and (c) wide spreaders.

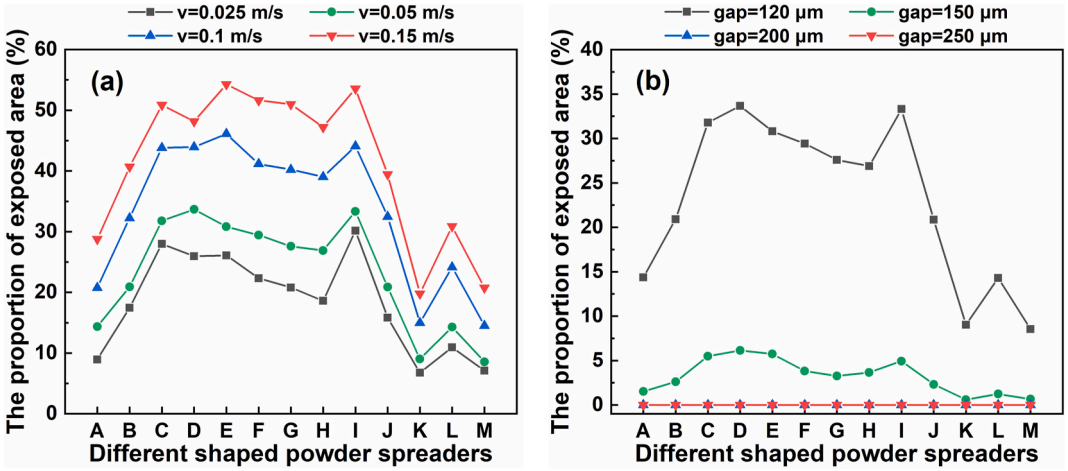

Fig. 12. Proportion of exposed area in the powder layer within the rough region for different spreaders: (a) different spreading speeds; (b) different layer gaps (spreaders A–E correspond to 30°, 45°, 90°, 120°, and 135°; spreaders F–H correspond to cut-blade, R30, and R60; spreaders I–M correspond to wideblade, cut-wideblade, R1000, R2000, and half-roundblade).

accumulation of particles, which increases the contact force between the particles. This action makes the particles adhere more tightly to the substrate surface, improving the powder coverage (Figs. 3 and 4). As the inclination angle increases, the force exerted by the spreader on the particles gradually becomes more uniform, reducing the degree of particle compression and accumulation. Consequently, the contact force decreases and stabilizes. This trend is particularly pronounced at inclination angles of 120° and 135° (Fig. 11(a)). For spreaders such as 90°, cut-blade, R30, and R60 (Fig. 11(b)), the bottom structures are similar, leading to minimal differences in the shear effects on the particles during the flow process. As a result, the contact forces between particles are relatively similar. However, for wide spreaders (Fig. 11(c)), the changes in bottom shape significantly affect the particle flow behavior. Spreaders with an arc-shaped bottom structure, such as R1000 and half-roundblade, promote better particle accumulation

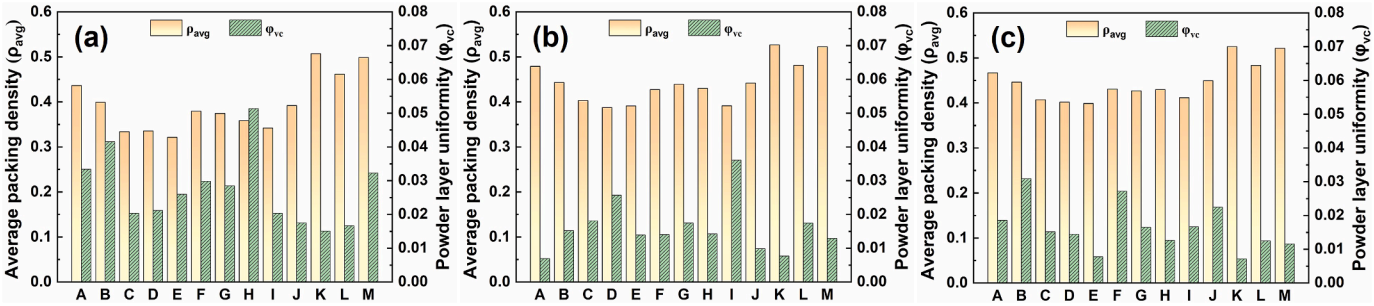

Fig. 13. Comparison of ρ_{avg} and φ_{vc} of powder layers formed by different spreaders in the rough region at different gaps: (a) 150 μm; (b) 200 μm; (c) 250 μm.

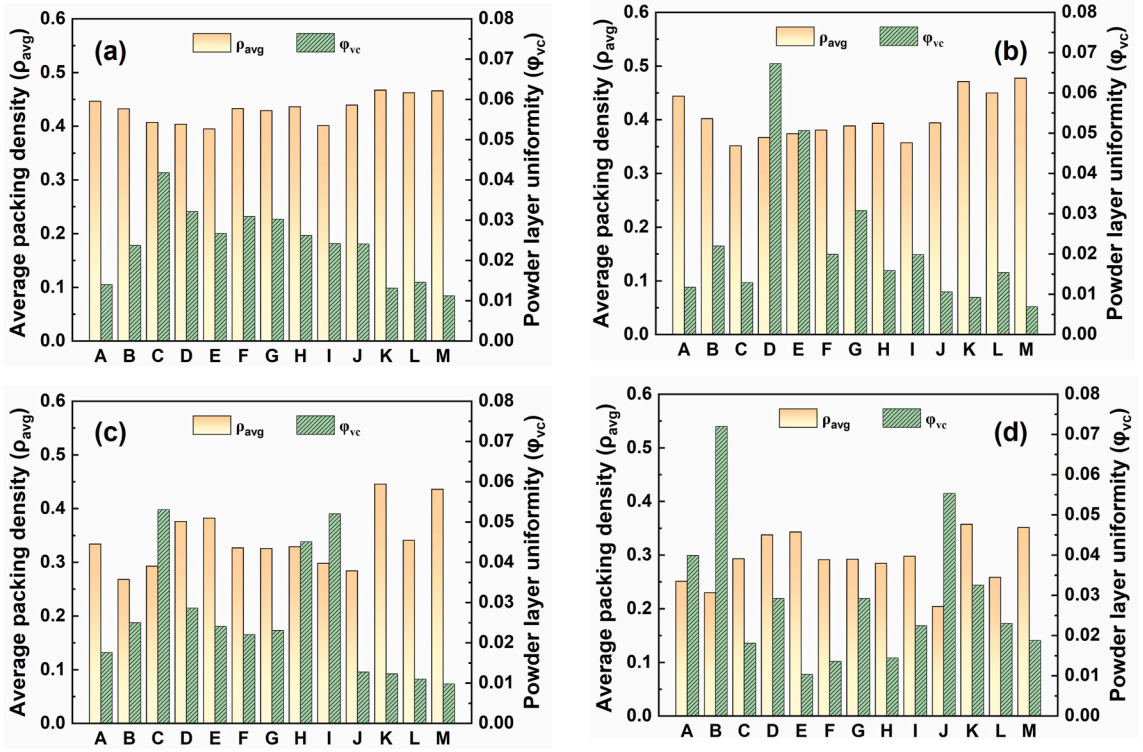

Fig. 14. Comparison of ρ_{avg} and φ_{vc} of powder layers formed by different spreaders in the smooth region at different spreading speeds: (a) 0.025 m/s; (b) 0.05 m/s; (c) 0.1 m/s; (d) 0.15 m/s.

and filling, resulting in larger contact forces. This, to some extent, enhances particle flow and uniform distribution. Therefore, R1000 and half-roundblade offer more significant advantages during the powder spreading process.

3.4. Influence of operational parameters on the powder spreading process

Spreading speed and layer gap are two important operational parameters. We carry out more simulations and analyze their effect under different spreading geometries. As shown in Fig. 12(a), with the increase in spreading speed, the area of uncovered regions in the powder bed generated by various spreaders shows a growing trend. Particularly, when the spreader inclination angle is less than 90°, the uncovered area increases significantly with the inclination angle. Among all spreaders, R1000 and half-roundblade consistently have the smallest proportion of uncovered areas in the powder bed, regardless of speed, demonstrating excellent spreading performance. Fig. 12(b) shows that when the layer gap reaches 200 μm, the exposed area in the powder bed disappears for all spreaders, indicating that a larger layer gap helps improve powder spreading uniformity. However, at smaller layer gaps, R1000 and half-roundblade still demonstrate the best spreading performance, with the smallest uncovered area. Furthermore, the study found that under different spreading speeds and layer gaps (e.g., gap = 120 μm and 150 μm), whether using narrow or wide spreaders, optimizing the bottom structure effectively reduces the uncovered area in the powder bed, thereby further improving spreading quality.

To further explore the evolution of powder bed performance in rough regions under varying layer gap conditions for different spreaders, Fig. 13 was plotted to illustrate the average packing density (ρ_{avg}) and uniformity (φ_{vc}) of the powder layer. As shown in Fig. 13, with the increase in layer gap, the average packing density of the powder bed generated by all spreaders shows an upward trend. When the spreader inclination angle is less than or equal to 90°, the average packing density decreases as the inclination angle increases, and this phenomenon does not change with the increase

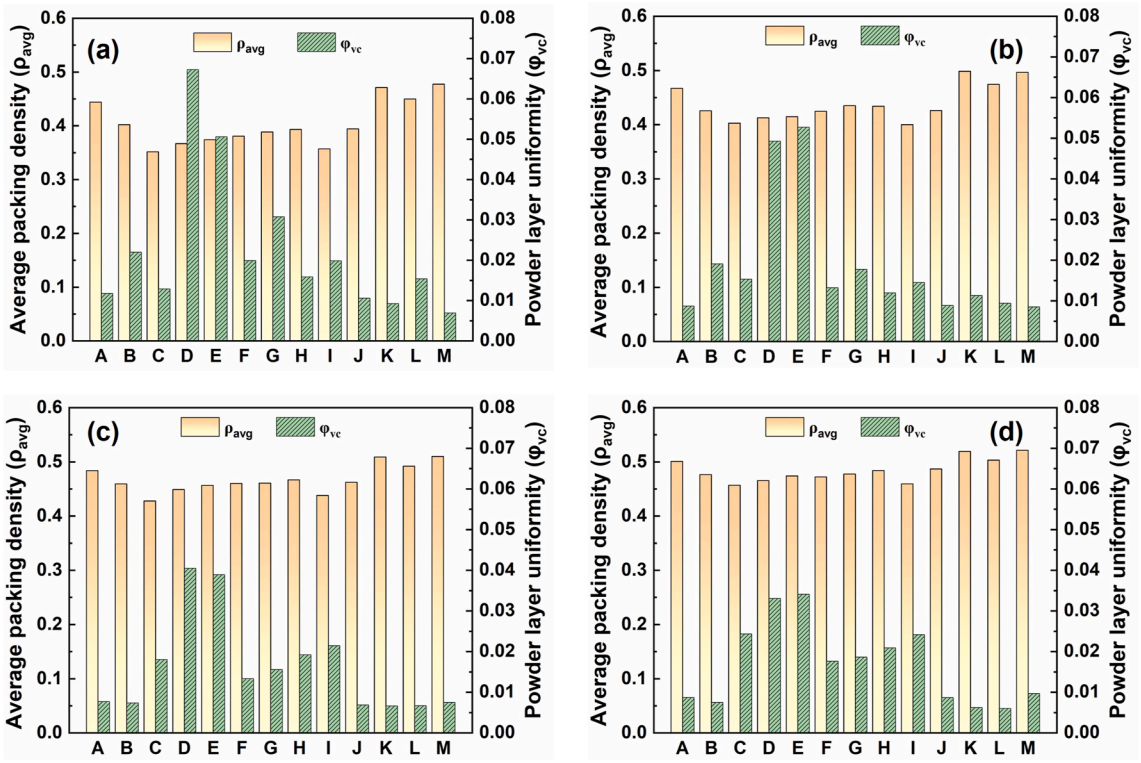

Fig. 15. Comparison of ρ_{avg} and φ_{vc} of powder layers formed by different spreaders in the smooth region at different gaps: (a) 120 μm; (b) 150 μm; (c) 200 μm; (d) 250 μm.

in layer gap. For narrow spreaders, the results show that as the layer gap increases, the powder layers generated by 90°, cut-blade, R30, and R60 gradually become more consistent. This indicates that the significant impact of narrow spreader types on packing density is mainly observed under low layer gap conditions, which is of great significance in practical processes. In contrast, for wide spreaders, optimizing the bottom structure allows for a higher average packing density under different layer gap conditions, demonstrating that the performance of wide spreaders is not significantly restricted by layer gap. Based on the analysis of both average packing density (ρ_{avg}) and uniformity (φ_{vc}), it can be concluded that the R1000 spreader outperforms all other spreaders in the rough region, exhibiting the best compactness and uniformity of the powder bed.

Additionally, this study also analyzed the powder bed characteristics of different spreaders on smooth surface regions under varying spreading speeds and layer gaps, as shown in Figs. 14 and 15. Fig. 14 demonstrates that as the spreading speed increases, the average packing density of the powder bed generated by all spreaders decreases significantly. When the spreader inclination angle does not exceed 90°, at lower spreading speeds (Fig. 14(a) and (b)), the packing density decreases with increasing inclination angle. However, this trend is disrupted at higher spreading speeds. Narrow spreaders (C, F–H) can enhance powder bed density through bottom structure optimization, but the effect is less pronounced at high spreading speeds. Among the wide spreaders, R1000 consistently improves packing density across all spreading speeds. At low spreading speeds, the half-roundblade produces a denser and more uniform powder bed. However, at high spreading speeds (Fig. 14(d)), its performance is worse than the spreader with the inclination angle of 135°. In Fig. 15, as the layer gap increases, the average packing density generated by each spreader also increases. On smooth surfaces, the powder bed density initially decreases and then increases with the increase in spreader inclination angle. Both narrow and wide spreaders with optimized bottom structures improve the powder bed density. When the layer gap is sufficiently large, the best-performing spreader shifts from half-roundblade to R1000.

4. Conclusions

DEM method is used in this work to simulate the powder spreading process of TC4 titanium alloy powder on rough substrate surfaces in the Laser Powder Bed Fusion (LPBF) process. The powder dynamics behavior of different spreaders under these conditions is investigated. By thoroughly analyzing the effects of various spreaders on powder spreading quality and flow behavior, the related patterns and underlying mechanisms are revealed. The main conclusions are as follows:

(1) With increasing the tilt angle of spreaders, the percentage of exposed area of the powder bed on the rough surface increases first from 14.4 % to 33.7 %, then decreases slightly to 30.8 %. While on the smooth surface, the amount of powder deposition shows a trend of decreasing and then increasing, with a slight decrease when the inclination angle reaches 135°. The powder bed quality on both surfaces can be effectively improved by optimizing the structure of the narrow spreader bottom or increasing the spreader thickness. However, the optimization of the wide spreader bottom structure (e.g. R1000 and R2000) is more effective. R1000 and half-roundblade perform best on both smooth and rough surfaces.
(2) During powder spreading, the direction of particle movement in the middle region of the powder pile approximately coincides with the direction of the texture of the rough surface at 45°. In addition, particle circulation occurs in the powder pile, and this circulation helps redistribute particles

on rough surfaces, improving the coverage. Larger contact forces between particles and the substrate help particles adhere more tightly to the surface, reduce inter-particle gaps, and stabilize particle positions, preventing local collapse and improving powder bed density. However, excessive force from the spreader can lead to tool wear and uneven spreading. Spreaders with arc-shaped structures improve packing density and distribution uniformity.

(3) On rough surfaces, when the spreader inclination angle is below 90°, powder bed packing density decreases with the angle increasing, regardless of the layer gap. Narrow spreaders increase the packing density at low layer gaps, while wide spreaders are not affected much. R1000 performs best in terms of compactness and uniformity. On smooth surfaces, with increasing the layer gap, the powder bed packing density initially decreases with increasing spreader tilt angle and then increases. As the layer gap increases, the best spreader changes from half-roundblade to R1000. At high spreading speed, R1000 and half-roundblade are the best spreaders for powder bed quality on rough surfaces, while on smooth surfaces, the spreader with the angle of 135° performs best.

CRediT authorship contribution statement

Yaping Wu: Writing – original draft, Validation, Methodology, Formal analysis, Visualization, Software, Investigation, Data curation. **Fuzhong Chu:** Supervision, Investigation, Writing – review & editing, Methodology, Conceptualization. **Chaocai Zhang:** Investigation, Writing – review & editing. **Hongyu Yan:** Investigation, Writing – review & editing. **Lin Wang:** Writing – review & editing, Software, Investigation, Supervision, Methodology, Conceptualization. **Zongyan Zhou:** Writing – review & editing, Validation, Software, Project administration, Investigation, Formal analysis, Visualization, Supervision, Resources, Methodology, Funding acquisition, Conceptualization.

Declaration of competing interest

The authors declare that they have no known competing financial interests or personal relationships that could have appeared to influence the work reported in this paper.

References

Ali, M. H., Sabyrov, N., & Shehab, E. (2022). Powder bed fusion–laser melting (PBF–LM) process: Latest review of materials, process parameter optimization, application, and up-to-date innovative technologies. *Progress in Additive Manufacturing, 7*(6), 1395–1422.

Bremen, S., Meiners, W., & Diatlov, A. (2012). Selective laser melting. *Laser Technik Journal, 9*(2), 33–38.

Cao, L. (2019). Study on the numerical simulation of laying powder for the selective laser melting process. *The International Journal of Advanced Manufacturing Technology, 105*(5), 2253–2269.

Cao, L. C., Li, J. C., Hu, J. X., Liu, H. P., Wu, Y. D., & Zhou, Q. (2021). Optimization of surface roughness and dimensional accuracy in LPBF additive manufacturing. *Optics & Laser Technology, 142*, Article 107246.

Chen, H., Wei, Q. S., Zhang, Y. J., Chen, F., Shi, Y. S., & Yan, W. T. (2019). Powder-spreading mechanisms in powder-bed-based additive manufacturing: Experiments and computational modeling. *Acta Materialia, 179*(15), 158–171.

Chu, F. Z., Li, E. L., Shen, H. P., Chen, Z. E., Li, Y. X., Liu, H., & Huang, A. J. (2023). Influence of powder size on defect generation in laser powder bed fusion of AlSi10Mg alloy. *Journal of Manufacturing Processes, 94*(26), 183–195.

Cundall, P. A., & Strack, O. D. L. (1979). A discrete numerical model for granular assemblies. *Géotechnique, 29*(1), 47–65.

Gao, X., Zhang, L. C., & Zhang, Z. (2024). Compatibility of tool geometry and process parameters in powder bed fusion. *Computational Particle Mechanics*.

Haeri, S. (2017). Optimisation of blade type spreaders for powder bed preparation in additive manufacturing using DEM simulations. *Powder Technology, 321*, 94–104.

Hamaker, H. C. (1937). The London—van der Waals attraction between spherical particles. *Physica, 4*(10), 1058–1072.

He, Y., Hassanpour, A., & Bayly, A. E. (2021). Combined effect of particle size and surface cohesiveness on powder spreadability for additive manufacturing. *Powder Technology, 392*, 191–203.

Hertz, H. (1882). *Uber die Berührung fester elastischer Körper(on the contact of elastic solids), 92*. De Gruyter.

Khairallah, S. A., Anderson, A. T., Rubenchik, A., & King, W. E. (2016). Laser powder-bed fusion additive manufacturing: Physics of complex melt flow and formation mechanisms of pores, spatter, and denudation zones. *Acta Materialia, 108*, 36–45.

Li, W., Liu, Q. P., Gao, Y. H., Chu, X. H., Zhang, Z., & Wang, Z. J. (2024). Investigation into SLM blade inclination effect on powder spreading behavior based on discrete element method. *Chinese Journal of Theoretical and Applied Mechanics, 56*(3), 774–784.

Li, W., Xu, K. N., H, Y., Hu, W. Y., & Wang, D. K. (2020). Numerical simulation of spreading process of lunar regolith simulant by DEM. *Journal of Beijing University of Aeronautics and Astronautics, 46*(10), 1863–1873.

Lifshitz, E. M., & Hamermesh, M. (1992). 26 - The theory of molecular attractive forces between solids. *Perspectives in Theoretical Physics*, 329–349.

Meier, C., Weissbach, R., Weinberg, J., Wall, W. A., & John, H. A. (2019). Modeling and characterization of cohesion in fine metal powders with a focus on additive manufacturing process simulations. *Powder Technology, 343*, 855–866.

Miao, G. X., Du, W. C., Pei, Z. J., & Ma, C. (2022). A literature review on powder spreading in additive manufacturing. *Additive Manufacturing, 58*, Article 103029.

Mindlin, R. D. (1949). Compliance of elastic bodies in contact. *Journal of Applied Mechanics, 16*(3), 259–268.

Mindlin, R. D., & Deresiewicz, H. (1953). Elastic spheres in contact under varying oblique forces. *Journal of Applied Mechanics, 20*(3), 327–344.

Murr, L. E., Gaytan, S. M., Ramirez, D. A., Martinez, E., Hernandez, J., Amato, K. N., & Wicker, R. B. (2012). Metal fabrication by additive manufacturing using laser and electron beam melting technologies. *Journal of Materials Science & Technology, 28*(1), 1–14.

Nan, W. G., & Gu, Y. Q. (2020). Investigation on the spreading dynamics of metal powder based on discrete element method. *The Chinese Journal of Process Engineering, 20*(11), 1313–1320.

Ngo, T. D., Kashani, A., Imbalzano, G., Nguyen, K. T. Q., & Hui, D. (2018). Additive manufacturing (3D printing): A review of materials, methods, applications and challenges. *Composites Part B: Engineering, 143*, 172–196.

Penny, R. W., Oropeza, D., Praegla, P. M., Weissbach, R., Meier, C., Wall, W. A., & John, H. A. (2024). Quantitative analysis of thin metal powder layers via transmission X-ray imaging and discrete element simulation: Blade-based spreading approaches. *Powder Technology, 432*, Article 119106.

Phua, A., Doblin, C., Owen, P., Davies, C. H. J., & Delaney, G. W. (2021). The effect of recoater geometry and speed on granular convection and size segregation in powder bed fusion. *Powder Technology, 394*, 632–644.

Qin, Y. C., Lou, S., Shi, P. Z., Qi, Q. F., Zeng, W. H., Scott, P. J., & Jiang, X. Q. (2024). Optimisation of process parameters for improving surface quality in laser powder bed fusion. *The International Journal of Advanced Manufacturing Technology, 130*(5), 2833–2845.

Roy, S., Xiao, H. Y., Angelidakis, V., & Pöschel, T. (2024). Combined thermal and particle shape effects on powder spreading in additive manufacturing via discrete element simulations. *Powder Technology, 445*, Article 120099.

Salehi, H., Cummins, J., Gallino, E., Garg, V., Deng, T., Hassanpour, A., & Bradley, M. (2023). Optimising spread-layer quality in powder additive manufacturing: Assessing packing fraction and segregation tendency. *Processes, 11*(8), 2276.

Sehhat, M. H., & Mahdianikhotbesara, A. (2021). Powder spreading in laser-powder bed fusion process. *Granular Matter, 23*(4), 89.

Si, L., Zhang, T. F., Zhou, M. Y., Li, M. Y., Zhang, Y., & Zhou, H. M. (2021). Numerical simulation of the flow behavior and powder spreading mechanism in powder bed-based additive manufacturing. *Powder Technology, 394*, 1004–1016.

Tsuji, Y., Tanaka, T., & Ishida, T. (1992). Lagrangian numerical simulation of plug flow of cohesionless particles in a horizontal pipe. *Powder Technology, 71*(3), 239–250.

Wang, L., Li, E. L., Shen, H., Zou, R. P., Yu, A. B., & Zhou, Z. Y. (2020). Adhesion effects on spreading of metal powders in selective laser melting. *Powder Technology, 363*, 602–610.

Wang, D., Yang, Y. Q., Liu, Y., Bai, Y. C., & Tan, C. L. (2023). Factors affecting the manufacturing quality of laser powder bed fusion. *Laser powder bed fusion of additive manufacturing technology*.

Wang, L., Yu, A. B., Li, E. L., Shen, H. P., & Zhou, Z. Y. (2021). Effects of spreader geometry on powder spreading process in powder bed additive manufacturing. *Powder Technology, 384*, 211–222.

Wang, L., Zhou, Z. Y., Li, E. L., Shen, H. P., & Yu, A. B. (2022). Powder deposition mechanism during powder spreading with different spreader geometries in powder bed fusion additive manufacturing. *Powder Technology, 395*, 802–810.

Wu, Q., Qiao, C., Wang, J., Yao, D. Z., Wu, Y. H., Fan, W., & An, X. Z. (2022). Adaptability investigations on bottom modified blade in powder spreading process of additive manufacturing. *Additive Manufacturing, 49*, Article 102477.

Xiang, Z. W., Yin, M., Deng, Z. B., Mei, X. Q., & Yin, G. F. (2016). Simulation of forming process of powder bed for additive manufacturing. *Journal of Manufacturing Science and Engineering, 138*(8), Article 081002.
Yao, D. Z., An, X. Z., Fu, H. T., Zhang, H., Yang, X. H., Zou, Q. C., & Dong, K. J. (2021). Dynamic investigation on the powder spreading during selective laser melting additive manufacturing. *Additive Manufacturing, 37*, Article 101707.
Zhao, C., Shi, B., Chen, S. L., Du, D., Sun, T., Simonds, B. J., & Rollett, A. D. (2022). Laser melting modes in metal powder bed fusion additive manufacturing. *Reviews of Modern Physics, 94*(4), Article 045002. Article 045002.